ADVANCED FUNCTIONAL MATERIALS
www.afm-journal.de

Stretchable and Self-Healable Semiconductive Composites Based on Hydrogen BondingCross-linked Elastomeric Matrix

Yunfei Wang, Kai-Lin Chen, Nathaniel Prine, Simon Rondeau-Gagné, Yu-Cheng Chiu, and Xiaodan Gu**

Semiconductors with both high stretchability and self-healing capability are highly desirable for various wearable devices. Much progress has been achieved in designing highly stretchable semiconductive polymers or composites. The demonstration of self-healable semiconductive composite is still rare. Here, an extremely soft, highly stretchable, and self-healable hydrogen bonding cross-linked elastomer, amide functionalized-polyisobutylene (PIB-amide) is developed, to enable a self-healable semiconductive composite through compounding with a high-performance conjugated diketopyrrolopyrrole (DPP-T) polymer. The composite, consisting of 20% DPP-T and 80% PIB-amide, shows record high crack-onset strain (COS ≈1500%), extremely low elastic modulus (E≈1.6 MPa), and unique ability to spontaneously self-heal atroom temperature within 5 min. Unlike previous works, these unique composite materials also show strain-independent charge mobility. An in-depth morphological study based on multi-model techniques indicate that all composites show blending ratio- and stretching-independent fibril-like aggregation due to the strong hydrogen bond in elastomer to enable the unique stable charge mobility. This study provides a new direction to develop highly healable and electronically stable semiconductive composite and will enable new applications of stretchable electronics.

1. Introduction

Developing stretchable and self-healable semiconductors is very important to meet the growing interest in designing wearable and implantable electronics.[1–8] Conjugated polymers (CPs), due to a wide range of tunable chemical structures and high flexibility and deformability compared to their inorganic counterparts, are widely adopted in wearable devices and used as the charge transport layer.[9–12] Unfortunately, a rigid and coplanar backbone and high crystallinity are preferred to enable effective charge transport for CPs, commonly rendering them as rigid and brittle.[13–15] Therefore, designing CPs with balanced electrical performance and mechanical robustness is required. Besides, mechanical fracture and accidental scratching in long-term use in daily life make the materials less durable.[8] In this regard, researchers developed a strong interest in making self-healing semiconductors or composites to mitigate above mentioned issues.[4–7,16]

Most efforts have focused on modifying chemical structures via backbone/side-chain engineering to develop stretchable and self-healable CPs. To improve stretchability, attaching longer, and branched alkyl side chains,[17–21] inserting flexible conjugation breaker spacers,[15,22–28] and copolymerizing soft segments with conjugated polymers[29–34] are generally used. However, the increased stretchability often resulted in sacrificed charge carrier mobility.[35] To introduce self-healing ability, dynamic covalent bonds (i.e., Diels–Alder reactions, imine bonds, disulfide exchanges, and borate ester bonds) or noncovalent interactions (i.e., hydrogen bonds,[24,36,37] metal–ligands interaction,[38] and host–guest interactions[39]) were often incorporated between the polymer chains. Despite considerable progress in developing self-healing polymeric materials,[40] only a few have focused on electronically active materials and demonstrated their usage in thin-film field-effect transistors. Besides, it must be noted that the molecular design of novel CPs always needs elaborate synthesis. Due to the conjugated nature of CP's rigid backbone, the demonstration of intrinsically stretchable and room temperature self-healable CPs is still limited.

Y. Wang, N. Prine, X. Gu
School of Polymer Science and Engineering
Center for Optoelectronic Materials and Devices
The University of Southern Mississippi
Hattiesburg, MS 39406, USA
E-mail: xiaodan.gu@usm.edu

K.-L. Chen, Y.-C. Chiu
Department of Chemical Engineering
National Taiwan University of Science and Technology
Taipei 106, Taiwan
E-mail: ycchiu@mail.ntust.edu.tw

S. Rondeau-Gagné
Department of Chemistry and Biochemistry
University of Windsor
Windsor, ON N9B3P4, Canada

The ORCID identification number(s) for the author(s) of this article can be found under https://doi.org/10.1002/adfm.202303031

DOI: 10.1002/adfm.202303031

Alternatively, physical blending CPs with soft elastomers (i.e., polydimethylsiloxane (PDMS),[41–44] styrene-ethylene-butylene-styrene (SEBS),[45–48] polystyrene-*block*-polyisoprene-*block*-polystyrene (SIS),[49] rubber,[50,51] etc.) is a straightforward and effective approach to create stretchable semiconductors.[44,45,55,46–48,50–54] For example, Bao et al. blended SEBS with poly(2,5–bis(2–octyldodecyl)–3,6–di(thiophen–2–yl)diketopyrrolo[3,4–c]pyrrole–1,4–dione–alt–thieno[3,2–b]thiophen (DPPT-TT) fabricating DPPT-TT/SEBS semiconducting composite.[48] Utilizing the conjugated polymer/elastomer phase separation-induced elasticity (CONPHINE) method, the high charge mobility of ≈1 $cm^2 V^{-1} s^{-1}$ was successfully retained even at 100% strain. Later on, the same group systematically studied the molecular weight (MW) influence of both CPs and SEBS on the performance of composites. For CPs with high MW, the aggregation slightly decreased upon increasing MW of SEBS, while the opposite trend was for CPs with low MW.[56] Furthermore, they also developed an elastic composite with the help of covalent cross-link between azide and C=C group in SEBS and C–C bond in CPs.[57] No residual strain showed up with increasing cyclic strains from 10% to 70%. Jeong et al. first used PDMS as elastomer matrix for the composites. The formation of poly(3–hexylthiophene–2,5–diyl) (P3HT) bundle networks in composite films enables high stretchability of composite (COS > 50%).[46] However, the mobility significantly decreased upon stretching. Cho group embedded P3HT nanowires into PDMS matrix.[42] The obtaining composites showed stable stretchability at strains up to 100%. Reichmanis group detailed studied processing condition effect on the performance of the P3HT/PDMS composite.[44] The one with "predeposition processed" P3HT showed 44 times higher hole mobility than the untreated one with high stretchability up to 100% strain. Apart from those previous demonstrations of the deformable composite, the self-healable capability for semiconductor composites is rarely demonstrated. Recently, Zhang et al. selected butyl rubber, an elastomer with high elasticity and strong adhesion, as the matrix to blend with poly(3,6–di(thiophen–2–yl)diketopyrrolo[3,4–c]pyrrolo–1,4–dione–alt–1,2–dithienylethene) (DPPTVT).[50] Although stretchability and self-healing capability was successfully achieved, a mismatch happened between the composite with blending ratio for the highest electrical performance and best mechanical stretchability. Jeong et al. embedded poly(3-butylthiophene-2,5-diyl) (P3BT) nanowires with dopant tris(pentafluorophenyl)borane (BCF) into thermoplastic elastomer matrix SIS fabricating SIS/P3BT/BCF composite. The obtained composites exhibited good thermoelectric performance, achieved self-healing under mild heat and pressure conditions, and good stretchability.[49] Oh, et al. fabricated metal–ligands cross-linked DPPTVT with 10 mol% 2,6–pyridinedicarboxamine moiedies (DPP-TVT-PDCA)/PDMS-PDCA composites.[58] With the dynamic metal–ligands interaction, the composites showed high stretchability (COS > 1300%) and self-healing ability. But the healing rate was relatively low, which needs 1 day to fully heal. Therefore, developing composites with both high stretchability and strong self-healing ability is of great interest to expand the application space for stretchable electronics.

To achieve the above goal, one can resort to the design of new high stretchable and self-healable elastomers with the needed properties for the semiconductive polymers. It's reported that polyisobutylene (PIB)-based networks have good flexibility and strong adhesion due to the softness and strong entanglement of the polymer chains.[59] Along this line, Higashihara incorporated PIB with P3HT synthesizing a block copolymer P3HT-*b*-PIB-*b*-P3HT. With the help of PIB segment, the obtained composite showed high stretchability with COS up to 200%.[60] Therefore, we expect PIB should own great potential to be used as an elastomer matrix to achieve stretchability and self-healing ability.

Introducing hydrogen bondingcross-link into elastomers was reported to improve stretchability and self-healing ability effectively.[61,62,71,63–70] The weaker dynamic bond is easy to break, providing an extra energy dissipation pathway to improve stretchability. After releasing stretching, the dynamic hydrogen bonds can reconnect again, enabling intrinsically self-healing abilities.[70] For example, Yan et al. utilized the ureidopyrimidinone (UPy) group to successfully construct a hydrogen bonding cross-linked supramolecular polymeric material (SPMs).[72] With the 20 mol% UPy group, an extremely stretchable material (COS = 17 000%) with excellent self-healing ability was obtained. Considering the excellent performance, hydrogen-bonding cross-linked elastomer should be a type of matrix with a high potential for stretchable and self-healable composites. However, far fewer advances have specifically addressed the availability of hydrogen bonding-cross-linked elastomers used in electronics and the influence of hydrogen bond on the performance of semiconducting composites.

Here, we designed a new hydrogen bonding cross-linked amide-functional PIB (PIB-Amide) to enable extremely soft, stretchable, and self-healable semiconductive composites, with PIB-Amide as the elastomer matrix, the semiconducting composite DPP-T/PIB-Amide exhibits blend ratio-independent mobility, with the extreme softness (E ≈ 1.76 MPa), high stretchability (COS ≈ 1500%), and strong self-healing ability at the room temperature (**Scheme 1**). In the meantime, the high charge carrier mobility of our composite can be mainly maintained under 100% cyclic strain for over 100 times. The properties were compared with reported semiconducting composites, which showed impressive improvement (Scheme 1d). Wide-angle X-ray scattering (WAXS), polarized UV–vis spectroscopy, and atomic force microscopic combined with infrared-spectroscopy (AFM-IR) were utilized to study the deformation mechanism. Through the in-depth morphology study, we conclude that the deformation happened mostly in the elastomer matrix while the network of the CPs fibril was connected throughout the stretching process, thus allowing the composite to maintain stable charge carrier mobility at different strains. This work demonstrated that CP/elastomer composites with hydrogen bonding cross-linked elastomer as the matrix can dramatically increase the stretchability and self-healing ability, which enriches the stretchable semiconductor materials choice and provides a guideline for the future design of stretchable and healable semiconductive composites.

2. Results and Discussion

Scheme 1 showed the overall design strategy of the extremely soft, stretchable, and self-healable semiconductor composites DPP-T/PIB-Amide. In our design, we engineered the non-covalent interactions into the elastomeric matrix. We expect the hydrogen bonding cross-link in elastomer can effectively improve

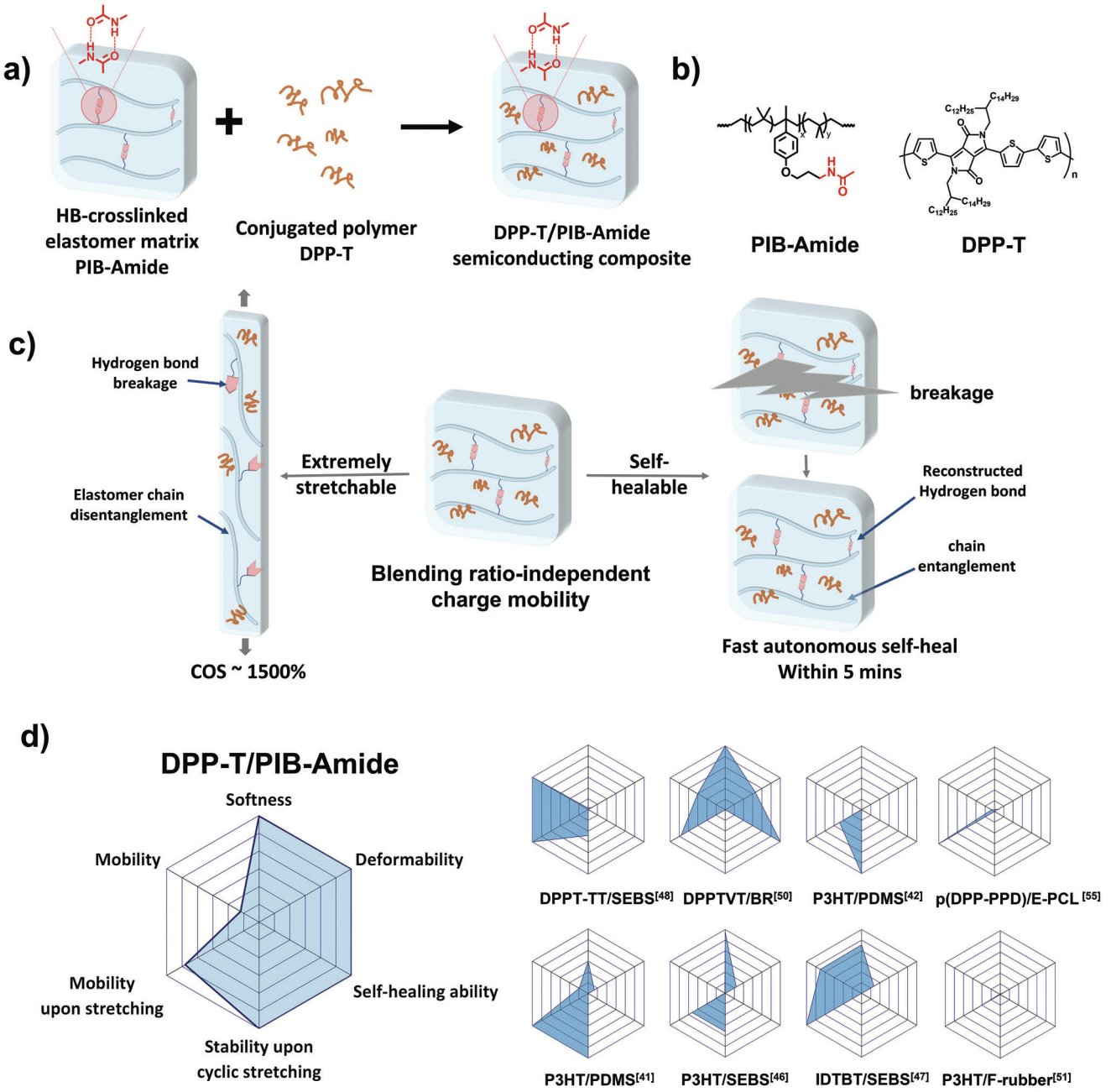

Scheme 1. a) Fabrication of DPP-T/PIB-Amide composite. b) Chemical structures of PIB-Amide and DPP-T. c) Schematic diagram showing the stretchable and self-healable DPP-T/PIB-Amide semiconducting composites. d) Comparison of the performance of the current system to previously reported semiconducting conjugated polymer/elastomer composites.

the composite's stretchability, self-healing ability, and charge carrier mobility. PIB-Amide was designed as the hydrogen bonding cross-linked elastomer matrix to take advantages of properties of PIB and non-covalent hydrogen bonding cross-link (**Scheme 2**). PIB is a soft and deformable elastomer with strong adhesion. Hydrogen bonding cross–link is an effective method to improve stretchability and self-healing ability. Combining these two components, the obtained PIB-Amide enables extreme softness (≈1 MPa), high stretchability (COS>1600%), and spontaneous self-healing ability at room temperature. The detailed synthesis and characterization of PIB-Amide were described in detail in Supporting Information (Figures S1–S7, Movie S1, Supporting Information). DPP-T was selected as the model CP because of the commercial availability and high charge mobility (μ ≈0.2 $cm^2 V^{-1} s^{-1}$, Figures S8 and S9, Supporting Information).

The blending ratio between CPs and elastomers was reported to significantly influence the electrical and mechanical properties of DPP-T/PIB-Amide composites.[50] We first studied the effect of the blend ratios (weight ratio of DPP-T at 0%, 10%, 20%, 30%, and 40% in the DPP-T/PIB-Amide composites)

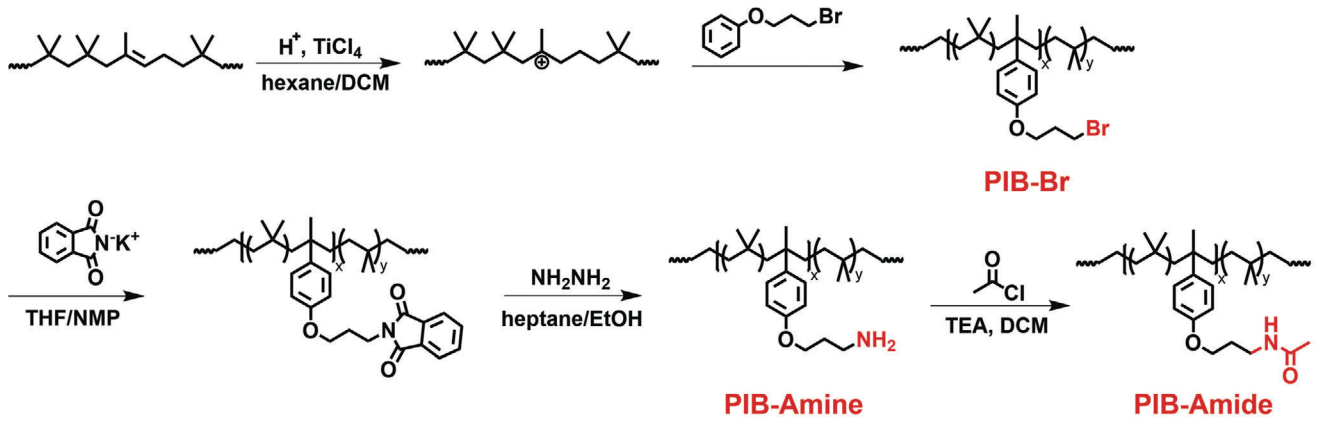

Scheme 2. Synthetic route of PIB-Amide.

on their physical and electrical properties. This blending ratio range is selected to ensure elastomer forms the matrix or continuous phase (weight ratio of CPs < 50%). A top-contact bottom-gate organic field-effect transistor (OFET) was fabricated to study the electrical properties of DPP-T/PIB-Amide composites (**Figure 1**a; Figures S10 and S11, Supporting Information). A fixed V_{sd} value of −60 V was used for all the transfer curve measurement. Notably, to avoid overestimating the electrical properties, the reliability factor of mobility calculations have substantiated exceeding 90%.[73] As a result, an average charge

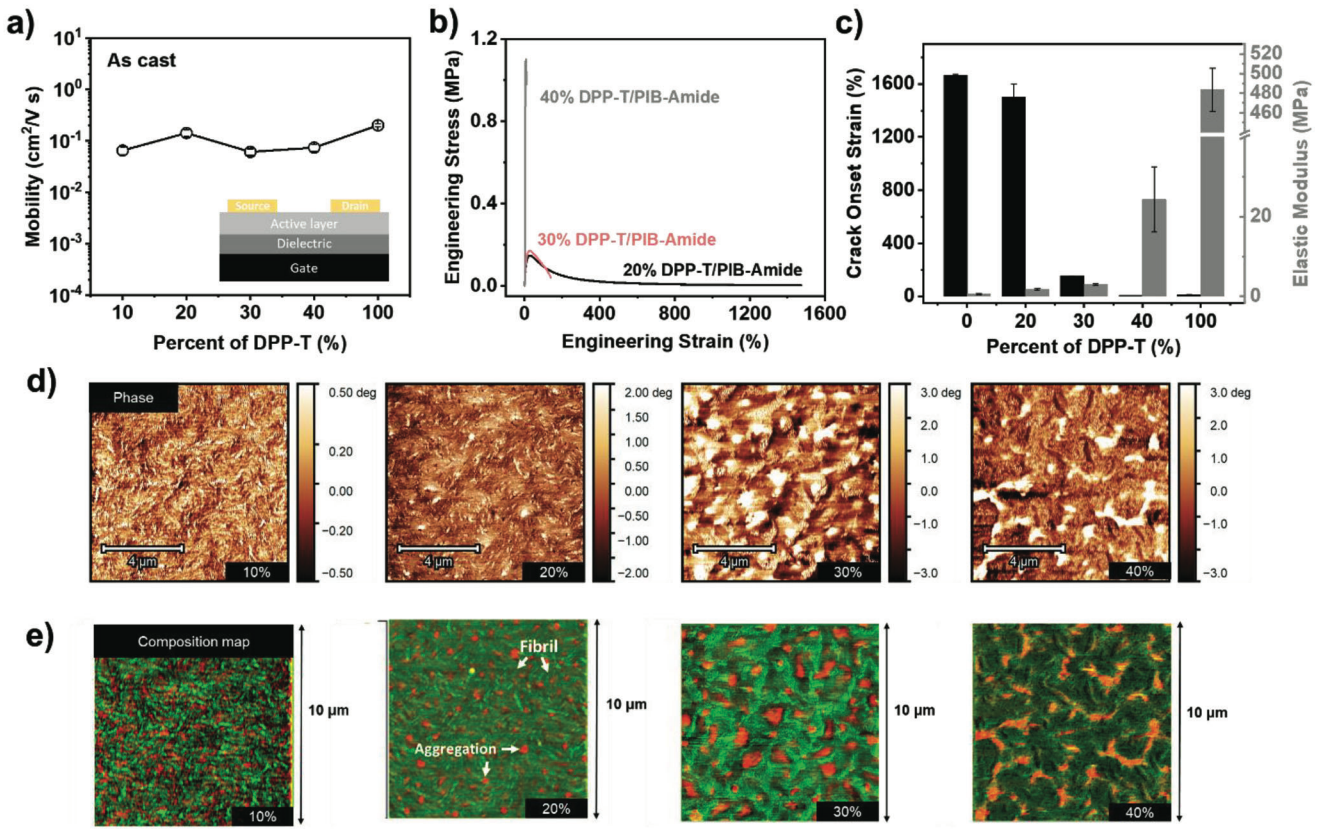

Figure 1. Mechanical, electrical, and morphology for DPP-T/PIB-Amide composite films with different blending ratios. a) Charge carrier mobility of 10–40% DPP-T/PIB-Amide composites and DPP-T thin films from top-contact bottom-gate OFET devices. b) Representative stress–strain curve of 20–40% DPP-T/PIB-Amide composite films. c) Elastic modulus and crack onset strain of 0, 20–40%, and 100% DPP-T/PIB-Amide composite films. d) AFM phase images of 10–40% DPP-T/PIB-Amide composite films. e) AFM-IR overlay images highlighting the distributions of DPP-T and PIB-Amide in 10–40% DPP-T/PIB-Amide composite films (red color represents DPP-T domain selectively excited using 1664 cm^{-1} laser, and green color represents for PIB-Amide domain selectively excited using 1462 cm^{-1} laser).

carrier mobility ≈0.09 cm^2 V^{-1} s^{-1} was observed for all 10–40% DPP-T/PIB-Amide composites, in which 20% DPP-T/PIB-Amide composite showed slightly higher average charge carrier mobility, ≈0.15 cm^2 V^{-1} s^{-1}. This stable charge mobility is attributed to fibril-like chain aggregation, which can exist in composites at different blending ratios, as will be discussed later. Pseudo-free standing tensile test was then performed to evaluate the mechanical properties of composites (Figure 1b,c; Figure S12 and Table S2, Supporting Information).[74,75] Sample composite films with 13 μm film thickness were prepared. 10% DPP-T/PIB-Amide composite absorbed water strongly, thus the data are not reported here. For the other three composites, 20% DPP-T/PIB-Amide showed a record highest COS of ≈1500% while maintaining a low E of 1.65 MPa. As the ratio of DPP-T increased, the COS continuously decreased to ≈7.67% (40% DPP-T/PIB-Amide) while E increased to 24.34 MPa, which was still much lower than pure DPP-T (483.62 MPa). Combining the aforementioned results, the blending ratio showed almost no effect on electrical properties but a significant influence on mechanical properties. 20% of DPP-T was determined to be the optimum blend ratio due to the highest stretchability and high charge carrier mobility, which was selected for further studies.

Morphology study was then performed to fully elucidate the observed mechanical and electrical properties using infrared-spectroscopy combined atomic force microscopy (AFM-IR) and grazing-incidence wide-angle X-ray scattering (GIWAXS). To obtain AFM-IR images, Fourier–transform infrared spectroscopy (FT-IR) was first performed on both pure CPs and elastomers to find a non-overlapping absorption peak for both components (Figure S13, Supporting Information). Comparing the absorption spectra of CPs and PIB-Amide, 1664 cm^{-1} (–C=O stretching vibration in amide) and 1462 cm^{-1} (–CH_2 torsional vibration in backbone) were chosen for selectively excited DPP-T and PIB-Amide, respectively. AFM tapping modes were then applied to obtain phase images (Figure 1d). After applying IR mode, two components can be clearly distinguished, and here they are labeled with two different colors (Figure 1e). The red and green regions represent the DPP-T and PIB-Amide, respectively. Both nanoscopic fibril-like aggregation from CPs and macro phase separation between CPs and PIB-Amide were observed for composites with all blending ratios. However, with an increased ratio of DPP-T, the macro-phase separation became more extensive, while fibril-like aggregation remained constant and well dispersed in rubber matrix. We attributed this blending ratio-independent fibril-like aggregation to hydrogen bonding cross-link between PIB. The hydrogen bond limits the chain mobility of elastomer, making the CP chains interact more with each other to form both the fibril and the large aggregation. The aggregation of CPs was reported beneficial to electrical properties of composites.[76,77] For example, Lee et al. added dimethylsulfoxide (DMSO) additive into poly(3,4–ethylenedioxythiophene) polystyrene sulfonate (PEDOT:PSS) that induces aggregation of PSS phase.[77] The aggregation effectively enhanced cohesion and electrical conductivity. Ouyang et al. studied other additives and observed similar phenomenon.[76] The formation of aggregation and enhanced conductivity were also observed with additive diethylene glycol (DEG) and poly(ethylene glycol) (PEG) 400. In terms of charge mobility in OFET applications, previous literature reports fibril-like CP aggregations in CP/elastomer composites contribute mostly.[78] Therefore, this explains that for four different composites, they all showed similar charge mobilities regardless of blending ratios. The morphology for bottom surface of the 20% DPP-T/PIB-Amide composite was also measured using AFM due to the significance for charge mobility, which showed a similar result as the top surface (Figure S14, Supporting Information). On the other hand, macro phase separation would lead to more rigid and brittle DPP phase due to their high modulus and low deformability. Therefore, with an increasing mixing ratio of DPP-T in composites, the E increased while deformability decreased. GIWAXS was then performed to study the crystallite structure of DPP-T domain in DPP-T/PIB-Amide composites (Figures S15 and S16, Table S3, Supporting Information). Similar values of lamella packing distance and FWHM were obtained, indicating that the blending ratio did not change the crystallite lattice packing, which also further provides insight to support the observed blending ratio-independent charge mobility.

The effect of hydrogen bonding cross–link on composites' electrical and mechanical properties was also studied using 20% DPP-T blended with various elastomer control samples (unmodified rubber, intermediate rubber product PIB-Br (Scheme 2) that does not have any hydrogen bonding functional groups, and hydrogen bonding cross-linked PIB-Amide) (Figures S17 and S18, Supporting Information). The synthesis of the PIB-Br can be found in supporting information as well.[79] The charge mobility of 20% DPP-T/BR, DPP-T/PIB-Br, and DPP-T/PIB-Amide was investigated. All composites performed similar charge mobilities, indicating that the hydrogen bond on elastomer didn't significantly influence the electrical properties (Figure S17a, Supporting Information). The effect of hydrogen bonds on mechanical properties was studied between 20% DPP-T/PIB-Br and DPP-T/PIB-Amide (Figures S17b and S18, Supporting Infprmation). The 20% DPP-T/PIB-Br showed COS of ≈400%, which was much lower than 20% DPP-T/PIB-Amide (COS≈1500%), demonstrating hydrogen bonding cross–link improved the stretchability of semiconducting composites due to the extra energy dissipation pathway provided by hydrogen bonds. Therefore, hydrogen bonding cross-link between elastomers can effectively improve the deformability of CP/elastomer semiconductor composites while maintaining device performance.

Maintaining electrical properties upon stretching and cyclic stretching plays a vital role in practical use. Next, the device's electrical properties under cyclic mechanical stretching were investigated. The study focused on using 150% strain. The composite sample was deposited onto the cross-linked elastic PDMS substrate. Then the bilayer sample was cyclically stretched using a motorized tensile stage. The charge mobility remains constant upon stretching (**Figure 2**a; Figures S19 and S22, Supporting Information). Furthermore, the high charge mobility value of the semiconductive composite can maintain over 100 repeated stretching cycles to 100% strain at 0.01 cm^2 V^{-1} s^{-1} (Figure 2b; Figures S23 and S24, Supporting Information). These results indicate the 20% DPP-T/PIB-Amide composites show high stability upon stretching and cyclic stretching, which is related to the stable crystallite structure as discussed below.

The deformation mechanism of 20% DPP-T/PIB-Amide composites was performed to understand the stable charge mobility using multi-model characterizations, including WAXS, polarized UV–vis absorption spectra, and AFM (**Figure 3**).[20] WAXS was

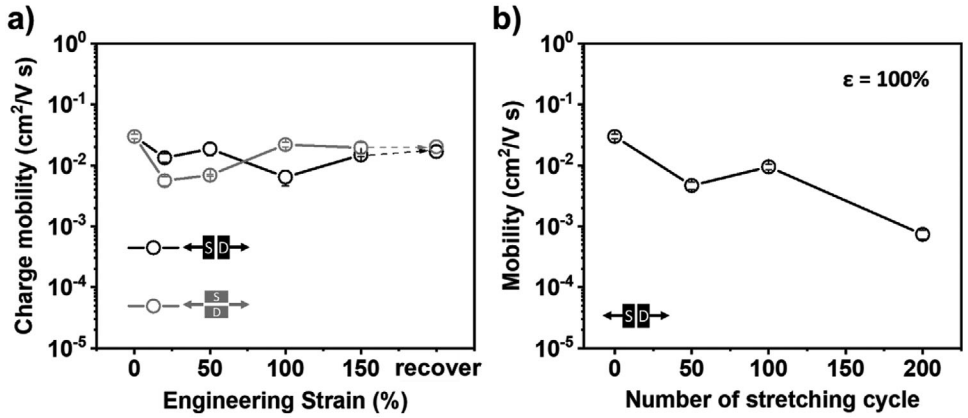

Figure 2. a) Charge carrier mobility of 20% DPP-T/PIB-Amide composites film upon stretching and recovery in parallel and perpendicular direction to charge transfer direction at different strains without annealing. b) Mobilities of 20% DPP-T/PIB-Amide composites film as a function of 100% strain stretching cycles parallel to the charge transport direction.

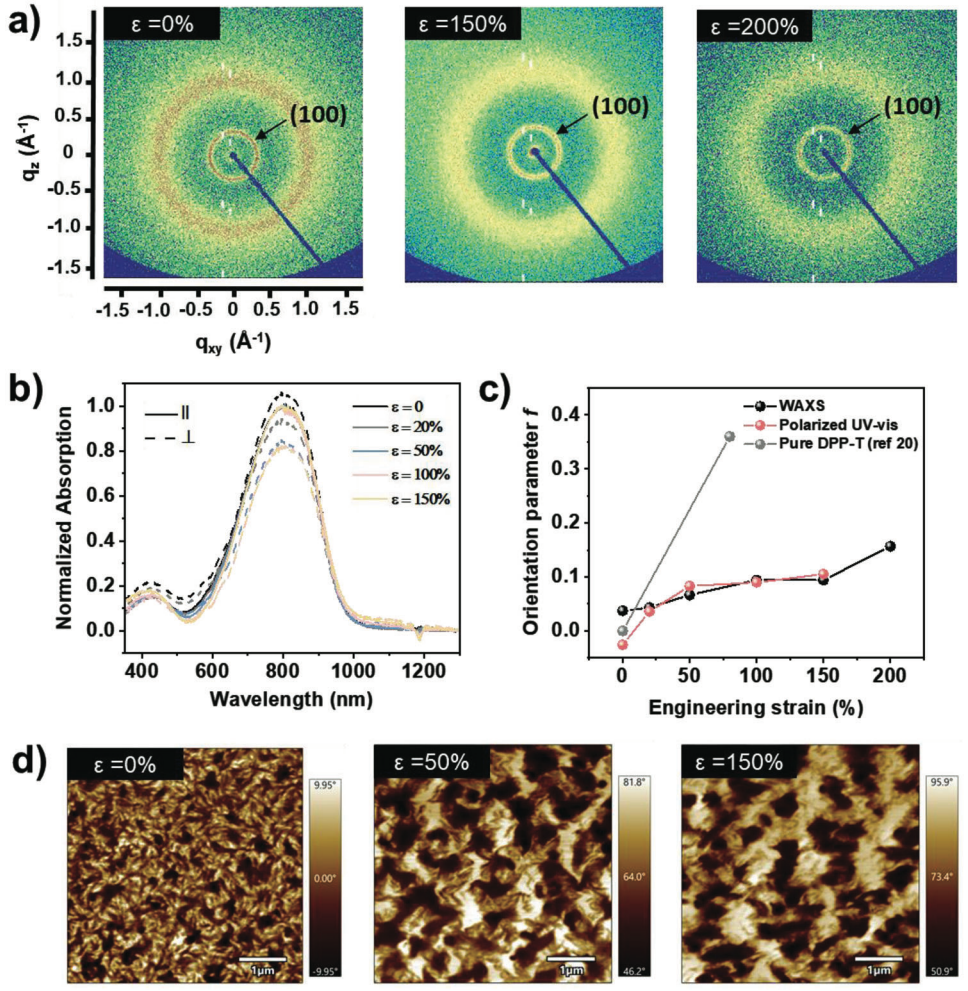

Figure 3. Deformation mechanism of 20% DPP-T/PIB-Amide composites. a) 2D scattering patterns of stretched 20% DPP-T/PIB-Amide composite films at 0%, 150%, and 200% strain from WAXS. b) Polarized UV–vis absorption plot of 20% DPP-T/PIB-Amide composite films at 0%, 20%, 50%, 100%, and 150% strain. c) Herman's orientation parameter *f* versus strain based on WAXS and polarized UV–vis. d) AFM phase images of stretched 20% DPP-T/PIB-Amide composite films at 0%, 50%, and 150% strains.

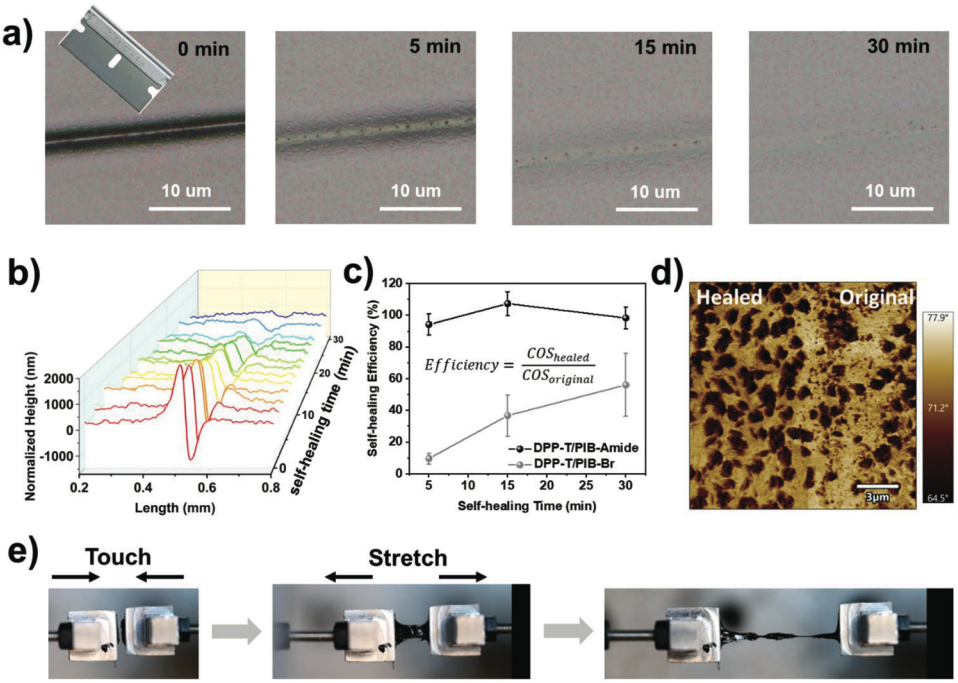

Figure 4. Self-healing ability of 20% DPP-T/PIB-Amide composite films. a) Optical microscope (OM) images of scratched semiconducting film through a self-healing process. b) Thickness map of scratched composite films through the self-healing process. c) Self-healing efficiency through the self-healing process. d) AFM phase images of healed composite films. e) Photographs of the self-healing process of composites from "cutting film" method.

first performed to investigate the crystallite domain alignment of DPP-T upon stretching. 2D scattering patterns and 1D line-cut profiles were shown in Figure 3a and Figures S25 and S26a (Supporting Information). From 2D scattering patterns, the (100) peak attributed to the lamellae packing peak was isotropic at the first 150% strain, indicating no obvious crystallite alignment. At 200% strain, the (100) peak began to become slightly anisotropic, demonstrating the crystallite packing direction started to rotate and align with the stretch direction. Orientation parameter f was calculated based on pole figure analysis of (100) peak to quantify the degree of crystallite alignment (Figure S26b, Supporting Information).[20] f showed a slight enhancement of 0.09 at the initial 150% strain and 0.16 at 200% (Figure 3c), indicating that the crystallite domain of DPP-T showed little alignment for the first 150% strain and moderate alignment at 200%. Besides, the lamellar packing distance and FWHM were calculated from WAXS of unstretched 20% DPP-T/PIB-Amide thick film (Table S4, Supporting Information), which was similar to the thin film from GIWAXS indicating the thickness of film didn't significantly influence the morphology. Polarized UV–vis was next to study the whole DPP-T polymer chain alignment. The normalized absorption spectrum for 20% DPP-T/PIB-Amide composite films under strain was plotted in Figure 3b, where peaks at ≈845 and 797 nm were assigned to the 0→0 and 0→1 peaks, respectively. Orientation parameter f change based on polarized UV–vis was calculated from the dichroic ratio, R, which was given by $f = (R-1)/(R+1)$. Orientation parameter f also slightly increased to 0.08 for 100% strain, which was much lower than the reported pure DPP polymer value ($f = 0.36$ at 100% strain).[20] Thus, the whole chain of DPP-T also only aligned a little. Combining results from WAXS and polarized UV–vis, we concluded that the high modulus CP component in composites almost didn't contribute to the first 150% strain, which supported the stable charge mobility upon stretching.

The impressive deformability of the semiconductive composite should be related to the soft elastomer domain, which should account for large strain upon stretching. To certify the contribution of the PIB-Amide component on stretched composites, AFM was performed (Figure 3d; Figure S27, Supporting Information). The white region, where there is higher phase shift in the tapping image, represents the softer elastomer phase, whereas the dark brown region represents high modulus DPP-T domains. At the strain of 150%, the white phase, PIB-Amide, and large DPP-T aggregation were stretched. In contrast, the fibril-aggregation remained constant, indicating that the deformation of elastomer and deformation of large DPP-T aggregation contributed most of the first 150% strain, agreed well with the results from WAXS and polarized UV–vis.

Self-healing ability is an important property allowing for the repair of local defects under cyclic mechanical stress for wearable devices in real life scenarios. Due to the self-healing ability of PIB-Amide, we expected the DPP-T/PIB-Amide composites should also perform strong self-healing abilities. The self-healing ability of 20% DPP-T/PIB-Amide composites was evaluated in two different methods, named "scratching film test" and "cutting film healing test" here, respectively. The scratching film method was first performed. In detail, a thick composite film was drop-casted onto a flat silicon wafer and scratched using a razor blade to introduce a scratch into the film (**Figure 4**a). The scratched composites were placed in an air environment without any additional thermal or solvent vapor treatment. To evaluate the self-healing ability, the gap change was monitored

using both optical microscopy (OM) and profilometer from 0 to 30 min after scratching (Figure 4a). The gap is quickly healed from OM images, where the scratch becomes lighter in color after 5 min and almost disappeared after 30 min. The thickness change of the gap was measured by profilometer to quantify the healing processing (Figure 4b). After scratching, a ≈1.5 µm crack was generated and became lighter and lighter within 30 min (≈1 µm for 8 min, 0.5 µm for 15 min, and 0.1 µm for 30 min). A tensile test was then performed to calculate the self-healing efficiency, given by the ratio of COS after self-healing and COS of unscratched composite films.[80] In 5 min, the self-healing efficiency of 20% DPP-T/PIB-Amide composite reached 94% and 100% after 15 min (Figure 4c). Therefore, the 20% DPP-T/PIB-Amide composite showed excellent self-healing ability. To demonstrate the mechanism of self-healing of 20% DPP-T/PIB-Amide composite, the self-healing efficiency of a control sample using non-hydrogen bonding cross-link composite (20% DPP-T/PIB-Br) was also measured (Figure 4c). The self-healing efficiency of DPP-T/PIB-Br composite film was 10% for 5 min and increased to 56% at 30 min indicating PIB itself has some healing ability due to the low glass transition temperature to promote local chain diffusion and chain entanglement. However, such capability is not on par with the composite using rubber matrix with hydrogen bonding cross-link, where the self-healing ability improved significantly. Therefore, the strong self-healing ability of 20% DPP-T/PIB-Amide composite is attributed to both the association effect of entanglement of PIB chains and hydrogen bonding cross-link. AFM was used to study morphology on the healed part. The healed film showed similar morphology but larger phase separation (Figure 4d).

The cutting film method is another method we used here to demonstrate the self-healing ability. Bulk composite films were first drop-cast on Si wafers. After immersing in liquid nitrogen, the bulk film was cut into two separate pieces. The separated pieces were pressed again for 25 s, followed by being stretched (See Movie S2, Supporting Information). The two parts successfully stuck and showed high stretchability, indicating the self-healing of DPP-T/PIB-Amide composites were very fast and strong (Figure 4e).

3. Conclusion

In summary, we successfully synthesized hydrogen bonding cross-linked elastomer, PIB-Amide, to fabricate a CP/elastomer composite with record highest crack-onset strain of 1500%, the low elastic modulus of 1.6 MPa, blending ratio-independent charge mobility of ≈0.09 $cm^2 V^{-1} s^{-1}$ and stable electrical properties upon cyclic stretching. Morphology study indicated the elastomer domain accommodated most of the strain upon stretching, allowing the electronic active conjugated polymer fibril phase to remain intact, allow maintaining a high and stable charge carrier mobility. The strong self-healing ability originates from the association effect of chain entanglement of PIB and the dynamic nature of hydrogen bonds. This work developed a new semiconducting composite with all-around high performance, which enriches the stretchable semiconducting polymer and provides a guideline for the future design of stretchable semiconductors.

Supporting Information

Supporting Information is available from the Wiley Online Library or from the author.

Acknowledgements

Y.W. and K.-L.C. contributed equally to this work. The authors thank the National Science Foundation under ward number DMR-2047689 for supporting this work. S.R.-G. thank the Natural Sciences and Engineering Research Council of Canada (NSERC) for financial support through a Discover Grant (RGPIN-2022-04428). K.-L.C. and Y.-C.C. thank the financial support from the Ministry of Science and Technology in Taiwan (MOST 111-2628-E-011-008-MY3). Work at the Molecular Foundry was supported by the Office of Science, Office of Basic Energy Sciences, of the U.S. Department of Energy under Contract No. DE-AC02-05CH11231. Y.W. was supported in part by an ALS Doctoral Fellowship in Residence. The authors thank Chih-Ting Liu and Dr. Lifeng Huang for assistance with device performance, Dr. Kyle Mehringer, Logan Dugas, Dana Pinson, and Dr. Robson Storey for the help with the synthesis of rubbery materials, Dr. Haoyu Zhao, Dr. Zhiqiang Cao, Dr. Song Zhang, and Dr. Luke A. Galuska for suggestions of morphology characterization.

Conflict of Interest

The authors declare no conflict of interest.

Data Availability Statement

The data that support the findings of this study are available from the corresponding author upon reasonable request.

Keywords

conjugated polymer/elastomer composites, hydrogen bonding cross-links, self-healable, stretchable

Received: March 17, 2023
Revised: May 30, 2023
Published online:

[1] D. H. Kim, N. Lu, R. Ma, Y. S. Kim, R. H. Kim, S. Wang, J. Wu, S. M. Won, H. Tao, A. Islam, K. J. Yu, T. Il Kim, R. Chowdhury, M. Ying, L. Xu, M. Li, H. J. Chung, H. Keum, M. McCormick, P. Liu, Y. W. Zhang, F. G. Omenetto, Y. Huang, T. Coleman, J. A. Rogers, *Science* **2011**, *333*, 838.
[2] D. J. Lipomi, Z. Bao, *MRS Bull.* **2017**, *42*, 93.
[3] D. Son, J. Lee, S. Qiao, R. Ghaffari, J. Kim, J. E. Lee, C. Song, S. J. Kim, D. J. Lee, S. W. Jun, S. Yang, M. Park, J. Shin, K. Do, M. Lee, K. Kang, C. S. Hwang, N. Lu, T. Hyeon, D. H. Kim, *Nat. Nanotechnol.* **2014**, *9*, 397.
[4] Z. Ma, H. Li, X. Jing, Y. Liu, H. Y. Mi, *Sens. Actuators, A* **2021**, *329*, 112800.
[5] S. Latif, S. Amin, S. S. Haroon, I. A. Sajjad, *Mater. Res. Express* **2019**, *6*, 062001.
[6] H. Yue, Z. Wang, Y. Zhen, *ACS Omega* **2022**, *7*, 18197.
[7] F. Mashkoor, S. J. Lee, H. Yi, S. M. Noh, C. Jeong, *Int. J. Mol. Sci.* **2022**, *23*, 622.
[8] L. Laysandra, A. Njotoprajitno, S. P. Prakoso, Y. C. Chiu, *Mater. Adv.* **2022**, *3*, 7154.

[9] K. Müllen, W. Pisula, *J. Am. Chem. Soc.* **2015**, *137*, 9503.
[10] S. Himmelberger, A. Salleo, *MRS Commun.* **2015**, *5*, 383.
[11] C. B. Nielsen, M. Turbiez, I. McCulloch, *Adv. Mater.* **2013**, *25*, 1859.
[12] H. N. Tsao, K. Müllen, *Chem. Soc. Rev.* **2010**, *39*, 2372.
[13] R. Noriega, J. Rivnay, K. Vandewal, F. P. V. Koch, N. Stingelin, P. Smith, M. F. Toney, A. Salleo, *Nat. Mater.* **2013**, *12*, 1038.
[14] H. Sirringhaus, M. Bird, T. Richards, N. Zhao, *Adv. Mater.* **2010**, *22*, 3893.
[15] S. E. Root, S. Savagatrup, A. D. Printz, D. Rodriquez, D. J. Lipomi, *Chem. Rev.* **2017**, *117*, 6467.
[16] J. Kang, J. B. H. Tok, Z. Bao, *Nat. Electron.* **2019**, *2*, 144.
[17] D. Liu, J. Mun, G. Chen, N. J. Schuster, W. Wang, Y. Zheng, S. Nikzad, J. C. Lai, Y. Wu, D. Zhong, Y. Lin, Y. Lei, Y. Chen, S. Gam, J. W. Chung, Y. Yun, J. B. H. Tok, Z. Bao, *J. Am. Chem. Soc.* **2021**, *143*, 11679.
[18] F. Sugiyama, A. T. Kleinschmidt, L. V. Kayser, D. Rodriquez, M. Finn, M. A. Alkhadra, J. M. H. Wan, J. Ramírez, A. S. C. Chiang, S. E. Root, S. Savagatrup, D. J. Lipomi, *Polym. Chem.* **2018**, *9*, 4354.
[19] H.-C. Yen, Y.-C. Lin, W.-C. Chen, *Macromolecules* **2021**, *54*, 1665.
[20] S. Zhang, A. Alesadi, G. T. Mason, K. L. Chen, G. Freychet, L. Galuska, Y. H. Cheng, P. B. J. St Onge, M. U. Ocheje, G. Ma, Z. Qian, S. Dhakal, Z. Ahmad, C. Wang, Y. C. Chiu, S. Rondeau-Gagné, W. Xia, X. Gu, *Adv. Funct. Mater.* **2021**, *31*, 2100161.
[21] Y. C. Chiang, H. C. Wu, H. F. Wen, C. C. Hung, C. W. Hong, C. C. Kuo, T. Higashihara, W. C. Chen, *Macromolecules* **2019**, *52*, 4396.
[22] J. Mun, G. J. N. Wang, J. Y. Oh, T. Katsumata, F. L. Lee, J. Kang, H. C. Wu, F. Lissel, S. Rondeau-Gagné, J. B. H. Tok, Z. Bao, *Adv. Funct. Mater.* **2018**, *28*, 1804222.
[23] S. Savagatrup, X. Zhao, E. Chan, J. Mei, D. J. Lipomi, *Macromol. Rapid Commun.* **2016**, *37*, 1623.
[24] J. Y. Oh, S. Rondeau-Gagné, Y. C. Chiu, A. Chortos, F. Lissel, G. J. N. Wang, B. C. Schroeder, T. Kurosawa, J. Lopez, T. Katsumata, J. Xu, C. Zhu, X. Gu, W. G. Bae, Y. Kim, L. Jin, J. W. Chung, J. B. H. Tok, Z. Bao, *Nature* **2016**, *539*, 411.
[25] Y. Zheng, M. Ashizawa, S. Zhang, J. Kang, S. Nikzad, Z. Yu, Y. Ochiai, H. C. Wu, H. Tran, J. Mun, Y. Q. Zheng, J. B. H. Tok, X. Gu, Z. Bao, *Chem. Mater.* **2020**, *32*, 5700.
[26] Y. Zhao, X. Zhao, Y. Zang, C. A. Di, Y. Diao, J. Mei, *Macromolecules* **2015**, *48*, 2048.
[27] X. Zhao, Y. Zhao, Q. Ge, K. Butrouna, Y. Diao, K. R. Graham, J. Mei, *Macromolecules* **2016**, *49*, 2601.
[28] Y. Zhao, X. Zhao, M. Roders, A. Gumyusenge, A. L. Ayzner, J. Mei, *Adv. Mater.* **2017**, *29*, 1605056.
[29] C. Müller, S. Goffri, D. W. Breiby, J. W. Andreasen, H. D. Chanzy, R. A. J. Janssen, M. M. Nielsen, C. P. Radano, H. Sirringhaus, P. Smith, N. Stingelin-Stutzmann, *Adv. Funct. Mater.* **2007**, *17*, 2674.
[30] K. Ditte, J. Perez, S. Chae, M. Hambsch, M. Al-Hussein, H. Komber, P. Formanek, S. C. B. Mannsfeld, A. Fery, A. Kiriy, F. Lissel, *Adv. Mater.* **2021**, *33*, 2005416.
[31] S. Zhang, M. U. Ocheje, L. Huang, L. Galuska, Z. Cao, S. Luo, Y. Cheng, D. Ehlenberg, R. B. Goodman, D. Zhou, Y. Liu, Y. Chiu, J. D. Azoulay, S. Rondeau-Gagné, X. Gu, *Adv. Electron. Mater.* **2019**, *5*, 1800899.
[32] K. Sato, Y. Hemmi, A. Kato, H. Matsui, K. Fuchise, T. Higashihara, *Polymer* **2022**, *252*, 124934.
[33] R. Peng, B. Pang, D. Hu, M. Chen, G. Zhang, X. Wang, H. Lu, K. Cho, L. Qiu, *J. Mater. Chem. C* **2015**, *3*, 3599.
[34] L. C. Hsu, S. Kobayashi, T. Isono, Y. C. Chiang, B. J. Ree, T. Satoh, W. C. Chen, *Macromolecules* **2020**, *53*, 7496.
[35] A. D. Printz, D. J. Lipomi, *Appl. Phys. Rev.* **2016**, *3*, 021302.
[36] M. Y. Lee, S. Dharmapurikar, S. J. Lee, Y. Cho, C. Yang, J. H. Oh, *Chem. Mater.* **2020**, *32*, 1914.
[37] X. Yu, C. Li, C. Gao, X. Zhang, G. Zhang, D. Zhang, *SmartMat* **2021**, *2*, 347.
[38] C. H. Li, C. Wang, C. Keplinger, J. L. Zuo, L. Jin, Y. Sun, P. Zheng, Y. Cao, F. Lissel, C. Linder, X. Z. You, Z. Bao, *Nat. Chem.* **2016**, *8*, 618.
[39] R. Yu, Y. Yang, J. He, M. Li, B. Guo, *Chem. Eng. J.* **2021**, *417*, 128278.
[40] J. H. Xu, C. Di Ding, P. Chen, L. H. Tan, C. B. Chen, J. J. Fu, *Appl. Phys. Rev.* **2020**, *7*, 031304.
[41] G. Zhang, S. Lee, E. Gutiérrez-Meza, C. Buckley, M. McBride, D. A. Valverde-Chávez, Y. H. Kwon, V. Savikhin, H. Xiong, T. J. Dunn, M. F. Toney, Z. Yuan, C. Silva, E. Reichmanis, *Chem. Mater.* **2019**, *31*, 6530.
[42] E. Song, B. Kang, H. H. Choi, D. H. Sin, H. Lee, W. H. Lee, K. Cho, *Adv. Electron. Mater.* **2016**, *2*, 1500250.
[43] G. Zhang, M. McBride, N. Persson, S. Lee, T. J. Dunn, M. F. Toney, Z. Yuan, Y. H. Kwon, P. H. Chu, B. Risteen, E. Reichmanis, *Chem. Mater.* **2017**, *29*, 7645.
[44] D. Choi, H. Kim, N. Persson, P. H. Chu, M. Chang, J. H. Kang, S. Graham, E. Reichmanis, *Chem. Mater.* **2016**, *28*, 1196.
[45] S. Nikzad, H. C. Wu, J. Kim, C. M. Mahoney, J. R. Matthews, W. Niu, Y. Li, H. Wang, W. C. Chen, M. F. Toney, M. He, Z. Bao, *Chem. Mater.* **2020**, *32*, 897.
[46] M. Shin, J. Y. Oh, K. E. Byun, Y. J. Lee, B. Kim, H. K. Baik, J. J. Park, U. Jeong, *Adv. Mater.* **2015**, *27*, 1255.
[47] D. Liu, Z. Ding, Y. Wu, S. F. Liu, Y. Han, K. Zhao, *Macromolecules* **2022**, *55*, 297.
[48] J. Xu, S. Wang, G. J. N. Wang, C. Zhu, S. Luo, L. Jin, X. Gu, S. Chen, V. R. Feig, J. W. F. To, S. Rondeau-Gagné, J. Park, B. C. Schroeder, C. Lu, J. Y. Oh, Y. Wang, Y. H. Kim, H. Yan, R. Sinclair, D. Zhou, G. Xue, B. Murmann, C. Linder, W. Cai, J. B. H. Tok, J. W. Chung, Z. Bao, *Science* **2017**, *355*, 59.
[49] Y. J. Jeong, J. Jung, E. H. Suh, D. J. Yun, J. G. Oh, J. Jang, *Adv. Funct. Mater.* **2020**, *30*, 1905809.
[50] S. Zhang, Y. Cheng, L. Galuska, A. Roy, M. Lorenz, B. Chen, S. Luo, Y. Li, C. Hung, Z. Qian, P. B. J. St Onge, G. T. Mason, L. Cowen, D. Zhou, S. I. Nazarenko, R. F. Storey, B. C. Schroeder, S. Rondeau-Gagné, Y. Chiu, X. Gu, *Adv. Funct. Mater.* **2020**, *30*, 2000663.
[51] Y. C. Chiang, C. C. Shih, S. H. Tung, W. C. Chen, *Polymer* **2018**, *155*, 146.
[52] P. Kulatunga, N. Yousefi, S. Rondeau-Gagné, *Chemosensors* **2022**, *10*, 201.
[53] L. Janasz, M. Borkowski, P. W. M. Blom, T. Marszalek, W. Pisula, *Adv. Funct. Mater.* **2022**, *32*, 2105456.
[54] S. Riera-Galindo, F. Leonardi, R. Pfattner, M. Mas-Torrent, *Adv. Mater. Technol.* **2019**, *4*, 1900104.
[55] H. Tran, V. R. Feig, K. Liu, H. C. Wu, R. Chen, J. Xu, K. Deisseroth, Z. Bao, *ACS Cent. Sci.* **2019**, *5*, 1884.
[56] A. Peña-Alcántara, S. Nikzad, L. Michalek, N. Prine, Y. Wang, H. Gong, E. Ponte, S. Schneider, Y. Wu, S. E. Root, M. He, J. B. H. Tok, X. Gu, Z. Bao, *Adv. Electron. Mater.* **2023**, 2201055, https://doi.org/10.1002/aelm.202201055.
[57] Y. Zheng, Z. Yu, S. Zhang, X. Kong, W. Michaels, W. Wang, G. Chen, D. Liu, J. C. Lai, N. Prine, W. Zhang, S. Nikzad, C. B. Cooper, D. Zhong, J. Mun, Z. Zhang, J. Kang, J. B. H. Tok, I. McCulloch, J. Qin, X. Gu, Z. Bao, *Nat. Commun.* **2021**, *12*, 5701
[58] J. Y. Oh, D. Son, T. Katsumata, Y. Lee, Y. Kim, J. Lopez, H. C. Wu, J. Kang, J. Park, X. Gu, J. Mun, N. G. J. Wang, Y. Yin, W. Cai, Y. Yun, J. B. H. Tok, Z. Bao, *Sci. Adv.* **2019**, *5*, eaav3097.
[59] M. Bag, S. Banerjee, R. Faust, D. Venkataraman, *Sol. Energy Mater. Sol. Cells* **2016**, *145*, 418.
[60] T. Higashihara, S. Fukuta, Y. Ochiai, T. Sekine, K. Chino, T. Koganezawa, I. Osaka, *ACS Appl Polym Mater* **2019**, *1*, 315.
[61] G. Tillet, B. Boutevin, B. Ameduri, *Prog. Polym. Sci.* **2011**, *36*, 191.
[62] S. Mavila, O. Eivgi, I. Berkovich, N. G. Lemcoff, *Chem. Rev.* **2016**, *116*, 878.
[63] K. P. Nair, V. Breedveld, M. Weck, *Macromolecules* **2008**, *41*, 3429.
[64] Y. Osada, J.-P. Gong, *Adv. Mater.* **1998**, *10*, 827.

[65] L. R. Rieth, R. F. Eaton, G. W. Coates, *Angew. Chem., Int. Ed.* **2001**, *40*, 2153.
[66] P. Song, H. Wang, *Adv. Mater.* **2020**, *32*, 1901244.
[67] K. E. Feldman, M. J. Kade, E. W. Meijer, C. J. Hawker, E. J. Kramer, *Macromolecules* **2010**, *43*, 5121.
[68] M. C. Stuparu, A. Khan, C. J. Hawker, *Polym. Chem.* **2012**, *3*, 3033.
[69] M. U. Ocheje, B. P. Charron, Y. H. Cheng, C. H. Chuang, A. Soldera, Y. C. Chiu, S. Rondeau-Gagné, *Macromolecules* **2018**, *51*, 1336.
[70] J. A. Neal, D. Mozhdehi, Z. Guan, *J. Am. Chem. Soc.* **2015**, *137*, 4846.
[71] R. J. Wojtecki, M. A. Meador, S. J. Rowan, *Nat. Mater.* **2011**, *10*, 14.
[72] X. Yan, Z. Liu, Q. Zhang, J. Lopez, H. Wang, H. C. Wu, S. Niu, H. Yan, S. Wang, T. Lei, J. Li, D. Qi, P. Huang, J. Huang, Y. Zhang, Y. Wang, G. Li, J. B. H. Tok, X. Chen, Z. Bao, *J. Am. Chem. Soc.* **2018**, *140*, 5280.
[73] H. H. Choi, K. Cho, C. D. Frisbie, H. Sirringhaus, V. Podzorov, *Nat. Mater.* **2017**, *17*, 2.
[74] S. Zhang, L. A. Galuska, X. Gu, *J. Polym. Sci.* **2022**, *60*, 1108.
[75] S. Zhang, M. U. Ocheje, S. Luo, D. Ehlenberg, B. Appleby, D. Weller, D. Zhou, S. Rondeau-Gagné, X. Gu, *Macromol. Rapid Commun.* **2018**, *39*, 1800092.
[76] L. Ouyang, C. Musumeci, M. J. Jafari, T. Ederth, O. Inganäs, *ACS Appl. Mater. Interfaces* **2015**, *7*, 19764.
[77] I. Lee, G. W. Kim, M. Yang, T. S. Kim, *ACS Appl. Mater. Interfaces* **2016**, *8*, 302.
[78] I. Angunawela, M. M. Nahid, M. Ghasemi, A. Amassian, H. Ade, A. Gadisa, *ACS Appl. Mater. Interfaces* **2020**, *12*, 26239.
[79] C. G. Campbell, R. F. Storey, *J. Polym. Sci., Part A Polym. Chem.* **2017**, *55*, 1991.
[80] Y. L. Rao, A. Chortos, R. Pfattner, F. Lissel, Y. C. Chiu, V. Feig, J. Xu, T. Kurosawa, X. Gu, C. Wang, M. He, J. W. Chung, Z. Bao, *J. Am. Chem. Soc.* **2016**, *138*, 6020.